Submitted to ApJ on May 24, 2012 — Accepted on July 17, 2012.
Preprint typeset using LaTeX style emulateapj v. 5/2/11

arXiv:1207.5975v1 [astro-ph.HE] 25 Jul 2012

THE TYPE IIB SUPERNOVA 2011DH FROM A SUPERGIANT PROGENITOR

Melina C. Bersten[1], Omar G. Benvenuto[2], Ken'ichi Nomoto[1], Mattias Ergon[3], Gastón Folatelli[1], Jesper Sollerman[3], Stefano Benetti[5], Maria Teresa Botticella[4], Morgan Fraser[6], Rubina Kotak[6], Keiichi Maeda[1], Paolo Ochner[5], Lina Tomasella[5]

[1] Kavli Institute for the Physics and Mathematics of the Universe, Todai Institutes for Advanced Study, University of Tokyo, 5-1-5 Kashiwanoha, Kashiwa, Chiba 277-8583, Japan
[2] Facultad de Ciencias Astronómicas y Geofísicas, Universidad Nacional de La Plata, Paseo del Bosque S/N, B1900FWA La Plata, Argentina
[3] The Oskar Klein Centre, Department of Astronomy, AlbaNova, SE-106 91 Stockholm, Sweden
[4]INAF-Osservatorio Astronomico di Capodimonte Salita Moiariello, 16 80131 - Napoli
[5]INAF-Osservatorio Astronomico di Padova, vicolo dell'Osservatorio 5, 35122 Padova, Italy and
[6]Astrophysics Research Centre, School of Mathematics and Physics, Queen's University Belfast, Belfast BT7 1NN

Submitted to ApJ on May 24, 2012 — Accepted on July 17, 2012.

ABSTRACT

A set of hydrodynamical models based on stellar evolutionary progenitors is used to study the nature of SN 2011dh. Our modeling suggests that a large progenitor star —with $R \sim 200\ R_{\odot}$—, is needed to reproduce the early light curve of SN 2011dh. This is consistent with the suggestion that the yellow super-giant star detected at the location of the SN in deep pre-explosion images is the progenitor star. From the main peak of the bolometric light curve and expansion velocities we constrain the mass of the ejecta to be $\approx 2\ M_{\odot}$, the explosion energy to be $E = 6 - 10 \times 10^{50}$ erg, and the ^{56}Ni mass to be approximately 0.06 $M_{\odot}$. The progenitor star was composed of a helium core of 3 to 4 $M_{\odot}$ and a thin hydrogen-rich envelope of $\approx 0.1\ M_{\odot}$ with a main sequence mass estimated to be in the range of 12–15 $M_{\odot}$. Our models rule out progenitors with helium-core masses larger than 8 $M_{\odot}$, which correspond to $M_{\rm ZAMS} \gtrsim 25\ M_{\odot}$. This suggests that a single star evolutionary scenario for SN 2011dh is unlikely.

Subject headings: hydrodynamics—supernovae: general — supernovae: individual: SN 2011dh

1. INTRODUCTION

Type IIb supernovae (SNe IIb) are transitional objects within the family of core-collapse SNe (CCSNe), as their spectroscopic classification evolves from Type II (i.e. with H lines), to type Ib (i.e. dominated by helium lines). SNe IIb were recognized as a new class with the discoveries of SN 1987K (Filippenko 1988) and SN 1993J (e.g. Nomoto et al. 1993; Filippenko 1997). As the rest of CCSNe—which includes H-rich types II-P and II-L, H-less type Ib, and He-less type Ic—, they are believed to arise from the violent death of stars with initial masses greater than 8 $M_{\odot}$. Massive stars may suffer considerable mass loss during their evolution, due to strong stellar winds or mass transfer to a binary companion. Therefore, the vast spectroscopic and photometric diversity observed among CCSNe is related to the ability of the progenitor star to retain its outermost layers before the explosion. Despite the efforts to improve our understanding of the progenitor of each subclass of CCSNe, many questions remain open. In this sense, the study of a very well-observed object can shed light on the nature of CCSNe and their massive progenitor systems.

SN 2011dh was discovered on May 31.893 by amateur astronomers and immediately confirmed by the Palomar Transient Factory (PTF) in the nearby spiral galaxy M51 (Griga et al. 2011; Silverman et al. 2011; Arcavi et al. 2011) which had also hosted three other CCSNe in the past 17 years. Strong constraints on the date of explosion, to better than 0.6 days were established using pre- and post-SN imaging (Arcavi et al. 2011). SN 2011dh was extensively monitored in a wide wavelength range, including early detections in radio and X-rays (Soderberg et al. 2012). It was classified as type IIb (Arcavi et al. 2011), a relatively rare subclass of CCSNe, based on the optical spectrum. Soon after discovery, a source was identified as a possible progenitor of SN 2011dh in archival, multi-band HST images (Maund et al. 2011; Van Dyk et al. 2011). Photometry of the source is compatible with a yellow super-giant (YSG) star.

The detection of pre-supernova (pre-SN) objects in high-resolution imaging has provided important information on the possible progenitors of several SNe. For SNe II-P, these observations confirm the red supergiant nature of the progenitor, as previously suggested by theory. An upper limit of $M_{\rm ZAMS} = 16.5 \pm 1.5\, M_{\odot}$ was suggested for this type of SNe (Smartt et al. 2009). However, such upper limit has been recently revised by Walmswell & Eldridge (2012). They found a higher value for the maximum mass of SN II-P progenitors of $M_{\rm ZAMS} = 21^{+2}_{-1}\, M_{\odot}$ when additional extinction due to dust produced in the red supergiant wind is taken into account. For other subtypes of CCSNe, detections have not been as common and only in a few cases have the progenitors been conclusively identified, e.g the type II-pec SN 1987A (Gilmozzi et al. 1987), the type IIb SN 1993J (Aldering et al. 1994; Maund et al. 2004), and the type IIn SN 2005gl (Gal-Yam et al. 2007).

To determine the main-sequence mass ($M_{\rm ZAMS}$) from pre-SN imaging, it is necessary to derive a luminosity and intrinsic colour from the photometry, and compare with some evolutionary track. This was done for SN 2011dh by Maund et al. (2011) and Van Dyk et al. (2011). But although both studies obtained consistent effective tem-

melina.bersten@ipmu.jp

perature and luminosity, and they employed the same evolutionary model, the derived $M_{\rm ZAMS}$ was different. Because color uncertainties are expected to arise from unknown mass-loss history of the progenitor, Maund et al. (2011) assumed only the luminosity was reliable, and derived $M_{\rm ZAMS} = 13 \pm 3\ M_\odot$ from the end point of the evolutionary track that matched the luminosity. Meanwhile Van Dyk et al. (2011) derived $M_{\rm ZAMS} = 17 - 19\ M_\odot$ by choosing the closest track that matches the luminosity and color of the source in the Hertzsprung-Russell (H-R) diagram although this point does not correspond with the final position of the star at the end of its evolution. Alternatively, Murphy et al. (2011) compared stellar population synthesis with the stellar association surrounding SN 2011dh to derive $M_{\rm ZAMS}$. Assuming that the stars in the vicinity of the SN are coeval, they concluded that the value of $M_{\rm ZAMS}$ is most likely close to the estimate of Maund et al. (2011).

Some authors have suggested that the YSG star detected in the pre-SN images is not the actual progenitor of SN 2011dh but its binary companion or even an unrelated object. These authors suggest, instead, that the exploding object was a compact star. The arguments for this are based, first, on the shock velocity derived from radio and sub-millimeter observations (Soderberg et al. 2012; Bietenholz et al. 2012; Krauss et al. 2012). The relatively high shock velocity found, $v_{\rm sw} \approx 0.1\,c$, would indicate a compact progenitor, or a type cIIb SN, in the scheme proposed by Chevalier & Soderberg (2010). The second argument for a compact progenitor was introduced by Arcavi et al. (2011) and is based on the quick decline of the optical light curve (LC) soon after the explosion, as compared with SN 1993J, along with a low temperature derived from an early-time spectrum, as compared with analytic expressions by Rabinak & Waxman (2011). Such a compact progenitor would be inconsistent with the YSG star identified by Maund et al. (2011) and Van Dyk et al. (2011), which is expected to have a radius of $\approx 270\,R_\odot$ (from $\log L = 4.92\ L_\odot$, $T_{\rm eff} = 6000\,K$, given $L = R^2\,T_{\rm eff}^4$ in solar units).

Early observations such as those available for SN 2011dh provide a unique opportunity to analyze the physical properties of the progenitor. In particular, one of the most direct ways to estimate the size of the progenitor is by modeling the LC during the cooling phase that occurs after the shock break-out and before the reheating by radioactive decay. Observations during this phase are very scarce due to its short duration and so they are very valuable. The studies described above do not present a specific modeling of the early light curve. With the aim of assessing the nature of the progenitor we set out to perform a more detailed modeling of the available observations.

A well-known method to estimate the properties of the progenitor object, as well as the explosion energy, and the amount and distribution of the radioactive material, is to compare the observations with predictions from hydrodynamical models. In this paper, we present a set of hydrodynamical models applied to stellar evolutionary progenitors that aim to elucidate the compact or extended nature of the progenitor of SN 2011dh, as well as the main physical parameters of the explosion. Our initial and LC models are presented in § 2. A comparison between models and observations is done in § 3. The global physical parameters are studied in § 3.1, and the sensitivity of the LCs on the initial radius is investigated in § 3.2. In § 4 we discuss the results and summarize our main conclusions § 5.

2. STELLAR AND SUPERNOVA MODELS

To study the nature of SN 2011dh we compare the observations with a set of hydrodynamical models applied to initial structures from stellar evolutionary calculations. Our supernova models are computed using a one-dimensional Lagrangian hydrodynamic code with flux-limited radiation diffusion (Bersten et al. 2011). The explosion itself is simulated by injecting a certain amount of energy near the center of the progenitor object, which produces a powerful shock wave that propagates through the progenitor transforming thermal and kinetic energy of the matter into energy that can be radiated from the stellar surface. During the propagation of the shock wave, explosive nucleosynthesis produces unstable isotopes of iron-group elements, mainly ^{56}Ni. The decay of $^{56}{\rm Ni} \longrightarrow {}^{56}{\rm Co} \longrightarrow {}^{56}{\rm Fe}$ produces energetic γ-rays and positrons that are thermalized, providing extra energy that contributes to power the LC. The code includes γ-ray transfer in gray approximation for any distribution of ^{56}Ni , assuming a constant value for the γ-ray opacity, $\kappa_\gamma = 0.06\,y_e\ {\rm cm^2 g^{-1}}$, where y_e is the number of electrons per baryon (Swartz et al. 1995). Note that this approximation is appropriate for typical SN conditions as it has been shown by Swartz et al. (1995) through comparison with Monte Carlo simulations. Nucleosynthesis is, however, not consistently calculated but it is included as a pre-explosion condition, assuming that the energy released does not contribute significantly to the dynamics of the explosion itself, and that it only effect is on the chemical structure (see Woosley & Weaver 1990; Arnett 1996, for further details of this assumption).

LCs of SNe IIb have been successfully reproduced using helium stars with a very thin hydrogen envelope ($\lesssim 1\,M_\odot$) as pre-SN models (Shigeyama et al. 1994; Woosley et al. 1994; Blinnikov et al. 1998). Therefore, we adopt the same type of model as input for our hydrodynamic calculations. The He core models were calculated by Nomoto & Hashimoto (1988) using a single-star evolutionary code that follows the evolution of the He core from He burning until the collapse of the core assuming solar initial abundance. The external H-rich envelope of the He core was replaced with the proper boundary conditions obtained from the hydrostatic and thermal equilibrium envelope models (Nomoto & Sugimoto 1972; Nomoto 1974). To take into account the thin hydrogen envelope, we smoothly attached a low-mass H-rich envelope in hydrostatic and thermal equilibrium to the He core. The presence of the external envelope significantly modifies the radius but not the mass of the progenitor.

Specifically, we employ four different initial models with He core masses of 3.3 $M_\odot$ (He3.3), 4 $M_\odot$ (He4), 5 $M_\odot$ (He5), and 8 $M_\odot$ (He8), which correspond to the stellar evolution of single stars with main-sequence masses of 12, 15, 18, and 25 $M_\odot$, respectively (see Sugimoto & Nomoto 1980; Tanaka et al. 2009, for the He core mass – main-sequence mass relation). Figure 1 shows the initial density profile as a function of radius for the He4 model and for models with different H-rich envelopes attached to the core of the He4 model. The latter models will be analyzed in § 3.2.

The chemical structure of these He stars before the explosion consists of a Fe core of $\approx 1.4\ M_\odot$, surrounded by concentric layers of Si-rich, O-rich, and He-rich material. For each of the initial models, explosive nucleosynthesis was calculated with a reaction network that includes 280 isotopes up to ^{79}Br (Hix & Thielemann 1996, 1999). The results of the nucleosynthesis depend on the progenitor mass and the kinetic energy of the explosion and they have already been presented in previous studies (Thielemann et al. 1996). An important characteristic of the models is the variation in the mass of the O-rich layer which goes from 0.2 $M_\odot$ for the He3.3 model to 3 $M_\odot$ for the He8 model. Therefore, the determination of the oxygen mass using late-time spectra may provide a constraint on the main-sequence mass of the progenitor (Kawabata et al. 2010).

In Section 3.1 we study the explosion models for the three least massive initial models (He3.3, He4, and He5), using several values of explosion energy, ^{56}Ni mass, and ^{56}Ni distribution. In this analysis the mixing of ^{56}Ni is modified from that of the nucleosynthesis calculations in order to explain the rising part of the observed LC, as frequently done to model the LC of SNe Ibc (e.g. see Shigeyama et al. 1994; Woosley et al. 1994; Blinnikov et al. 2000). Such a mixing between the core and the He layer in Type Ib and IIb supernovae is caused by the Rayleigh-Taylor instability at the base of the He layer (Hachisu et al. 1991, 1994; Iwamoto et al. 1997). Actually, more recent 3D numerical calculations predict even larger mixing of ^{56}Ni than previous 2D calculations (Hammer et al. 2010; Joggerst et al. 2010). This result is in better agreement with the extensive mixing observed in e.g. SN 1987A. In Section 3.2 we study the effect of the external H-rich envelope which must be present to explain the H spectral features observed at early times. Finally, the He8 model is discussed in Section 4 to test the plausibility of a massive single progenitor star.

3. LIGHT CURVE MODELING

The g'-band LC of SN 2011dh showed a quick decline during 1–3 days after an initial peak with $M_g^{\rm peak} = -16.5$ mag. This initial decline was followed by a re-brightening in all bands leading to a second peak with bolometric luminosity of $L_{\rm bol} \approx 1.4 \times 10^{42}$ erg s^{-1} ($M_{\rm bol} = -16.6$ mag) at $t \approx 20$ days. Double-peaked LC have been observed for very few SNe, one of which was the well-known SN 1993J, although with a slower initial decline and larger luminosity, as compared with SN 2011dh. The scarcity of observations during the early declining phase is due to its very short duration, which makes it difficult to catch. Theoretically, however, all CCSNe should present this early behavior which is a consequence of cooling after the shock breaks out from the surface of the object. The duration of the cooling phase is mainly regulated by the size of the progenitor, although there is also a dependence on energy, mass and envelope composition. More compact structures, such as Wolf-Rayet stars, produce faster declines than extended progenitors, such as red supergiants.

On the other hand, the heat source that powers the second peak is provided by the radioactive decay of ^{56}Ni produced during the explosive nucleosynthesis and its daughter ^{56}Co. Modeling the LC around the second peak provides information about the explosion energy (E), ejecta mass ($M_{\rm ej}$), and the mass and distribution of ^{56}Ni . Such global properties for SN 2011dh are analyzed in Section 3.1 while the effect of the progenitor radius which essentially affects the early decline phase of the LC is studied in Section 3.2.

The observed bolometric LC of SN 2011dh and the expansion velocities for the Fe II lines used in this paper are taken from Ergon et al. (2012). A distance of 7.1 Mpc (Takáts & Vinkó 2006), a Galactic reddening of $E(B-V) = 0.035$ mag and no host-galaxy reddening (Arcavi et al. 2011) were assumed in the calculations. For the early cooling phase, there are only a few observations available in a limited wavelength range, which prevents us from calculating a bolometric luminosity during that epoch. Hence we directly adopt the g'-band data published by Arcavi et al. (2011). In the present work we assume the explosion time was 2011 May 31.5 UT, that is the mid-point between the last non-detection and the discovery date.

3.1. *Global properties of SN 2011dh*

To estimate physical parameters, such as explosion energy (E), ejected mass ($M_{\rm ej}$), and the mass (^{56}Ni mass) and distribution of ^{56}Ni, we analyze the bolometric LC around the second peak, and the photospheric velocitiy ($v_{\rm ph}$) evolution. For this purpose, the He star models presented in section 2 are adopted as initial configurations. To save computation time, no external H envelope was added at this point because this does not affect the LC around the main peak. Therefore, the progenitor is assumed to be compact with a radius of $R \approx R_\odot$.

First we analyze the general dependence of the LC and $v_{\rm ph}$ on variations of the physical parameters for model He4. This is the He core used by Shigeyama et al. (1994) to model the bolometric LC of SN 1993J with $E \approx 1.2$ foe (1 foe= 1×10^{51}erg), ^{56}Ni mass of $\sim$0.08 $M_\odot$, and assuming substantial mixing of ^{56}Ni out to the He layers (see also our own model of SN 1993J in Figure 12, Section 4.2). Following that work, for SN 2011dh we test physical parameters near those values.

Figures 2 and 3 show the effect of the explosion energy on the LC and on $v_{\rm ph}$, respectively, for energies of $E =$ 0.8, 1.0, and 1.5 foe. More energetic explosions produce larger kinetic and radiative energy, which is reflected in higher photospheric velocity and global brightness. After the cooling phase, all LCs evolve through a minimum with luminosity $L_{\rm min}$, followed by a broad second peak with maximum luminosity $L_{\rm peak}$, and then they enter a more or less linear decline, or "tail" phase. In the following analysis we denote the epochs of $L_{\rm min}$ and $L_{\rm peak}$ as $t_{\rm min}$ and $t_{\rm peak}$, respectively. From Figure 2 we see that $L_{\rm min}$ and $L_{\rm peak}$ increase with E while the luminosity during the tail phase shows a dependence in the opposite direction. Note that $t_{\rm min}$ is more or less independent of explosion energy, but $t_{\rm peak}$ decreases with E. Finally, models with lower E produce broader second peaks.

The effect of the ^{56}Ni mass on the LC is shown in Figure 4 for ^{56}Ni mass = 0.05, 0.06, and 0.07 $M_\odot$. The LCs are remarkably equal until about 10 days before $t_{\rm peak}$

when the models begin to differ in the sense that larger ^{56}Ni mass produces larger luminosity and wider LC. $L_{\rm peak}$ and the tail luminosity increase with ^{56}Ni mass but no appreciable effect is seen in $L_{\rm min}$. Also note that $t_{\rm min}$ and $t_{\rm peak}$ are essentially insensitive to the amount of synthesized ^{56}Ni.

The distribution of ^{56}Ni could be different than the one predicted by one-dimensional nucleosynthesis calculations where it is concentrated in the inner regions of the progenitor. Mixing of ^{56}Ni out to the helium envelope is expected to occur because of Rayleigh-Taylor instabilities during the propagation of the shock wave which are not properly taken into account in our one-dimensional prescription. To study the effect of mixing, we calculated three models with ^{56}Ni linearly mixed (in mass coordinate) out to 75% (He4Mix75), 85% (He4Mix85), and 95% (He4Mix95) of the total initial mass. Note that the distributions of ^{56}Ni adopted are in good concordance with recent 3D calculations (see e.g. Fig. 6 of Hammer et al. 2010).

The resulting LCs are shown in Figure 5. The main effect of mixing is seen at $t < t_{\rm peak}$ although there is also a smaller effect on the tail luminosity. For more extensive mixing, $t_{\rm min}$ is produced at earlier times because of the earlier heating by radioactive decay. This also produces a higher $L_{\rm min}$, while the value of $L_{\rm peak}$ seems not to be very sensitive to mixing. Instead the effect is more visible for the LC width which increases with more extended mixing.

The results of these tests show that the effect on $v_{\rm ph}$ of the ^{56}Ni mass and distribution is essentially negligible. Therefore, the kinetic energy available in the ejecta is the only relevant parameter that determines the photospheric velocity evolution, which imposes strict constraints on E for a given $M_{\rm ej}$.

This comparative analysis allows us to find a set of parameters that reproduce the observations of SN 2011dh. For He4, these parameters are $E = 1$ foe, and ^{56}Ni mass $= 0.065\ M_\odot$, mixed out to 95% of the total mass or out to 9000 km s^{-1} in velocity space. Note that although ^{56}Ni was mixed far out in the ejecta, since the adopted mixing function was linear, the amount of ^{56}Ni in the outer layers was small ($< 1.3 \times 10^{-3}\ M_\odot$ for $v >$ 5000 km s^{-1}). We adopted a cut mass ($M_{\rm cut}$) of 1.5 $M_\odot$ that is assumed to form a compact remnant. Therefore, the mass of the ejecta is $M_{\rm ej} = M_{\rm total} - M_{\rm cut} = 2.5 M_\odot$. A summary of the parameters used in this and the following calculations is presented in Table 1, where we show the main-sequence mass, He core mass, and radius of the progenitor, the mass cut assumed, the ejecta mass, the explosion energy and the ^{56}Ni mass.

We also tested the He3.3 and He5 models with smaller and larger pre-SN mass, respectively. The parameters found for these cases are slightly different from those of the He4 model (see Table 1), although the ^{56}Ni mixing was kept up to 95% of the total mass. For instance, in order to keep the agreement with the observed velocities, we modified the explosion energy so that the ratio $E/M_{\rm ej}$ remains approximately constant. Figures 6 and 7 show the LCs and $v_{\rm ph}$, respectively, for the parameters of models He3.3, He4, and He5 compared with the observations. From the figures, it is clear that the three models give good fits to the observations, with the two least massive ones producing slightly better results.

Models He3.3 and He4 give the best fits to velocity and LC, respectively. This means that there is a slight tension in the solution of the progenitor properties based on the comparison of our calculations with these observables. However, given the uncertainties involved, it is likely that the best global fit arises from a model with parameters in the range of these two models. That is, $M_{\rm ej} = 1.8$–2.5 $M_\odot$, $E = 0.6$–1.0 foe, and ^{56}Ni mass $= 0.060$ –0.065 $M_\odot$ mixed out to a velocity of ≈ 9000 km s^{-1}. Such a progenitor with a He core mass between 3 and 4 $M_\odot$ corresponds to a star of ≈ 12–15 $M_\odot$ on the main sequence. Although there are uncertainties in the determination of the main sequence mass from the He core mass, depending for example on convective overshooting, rotation, etc., for the range of He core masses considered here different stellar calculations provide similar results (see Figure 1 of Tanaka et al. 2009). Stars of such initial masses have no known mechanism to almost completely remove the H envelope, as required for producing a SN IIb, except through binary interaction. In Section 4 we study the possibility of more massive progenitors and discuss the binary scenario.

3.2. *Progenitor radius*

To test the effect of the progenitor radius on the LC, it is critical to obtain observations during the adiabatic cooling phase before the radioactive decay becomes the main source to power the LC. For the case of SN 2011dh, only a few data points in the g'-band are available at those times. Here we compare these data with two hydrodynamical models: a compact one with an initial radius of $\approx 2\ R_\odot$, and an extended one with $R \approx 270\ R_\odot$, consistent with the L and $T_{\rm eff}$ of the YSG star detected in pre-SN images. Both models have a He core mass of 4 $M_\odot$ and the same physical parameters as model He4 (see Table 1). The extended model (He4R270) was constructed by smoothly attaching to the helium core a H/He envelope in hydrostatic and thermal equilibrium (see Figure 1). The mass ($M_{\rm env}$) and the helium mass fraction (Y) of the envelope for a uniform composition were fit so that the L and $T_{\rm eff}$ became equal to the estimate from pre-SN imaging. This yielded values of $M_{\rm env} = 0.1\ M_\odot$ and $Y = 0.8$. Note that the total H mass in this model is $\approx 0.02\ M_\odot$, similar to the value derived from spectral modeling (Arcavi et al. 2011).

Figure 8 (left panel) shows the bolometric LCs for both the compact and the extended progenitor models. The effect of radius is only noticeable before $t \approx 5$ days, which is roughly where the bolometric LC data begin. At $t \sim 1$ day the difference in bolometric luminosity between the two models is very large, of up to one order of magnitude. This difference is mostly due to the extra amount of energy required to expand a more compact structure. Fortunately, earlier data obtained in the g' band are available to discriminate between the two models. Therefore, to compare with the g'-band data we calculated synthetic LCs assuming black-body emission and integrating the flux through the corresponding filter transmission function. Figure 8 (right panel) shows a comparison of our models with the g'-band observations for compact (blue line) and extended (red line) progenitors. Again, both models differ significantly in the g' band at $t < 5$ days. While the extended model produces a pronounced spike, in agreement with the observations, the compact progenitor shows a much weaker bump. From this analysis we conclude that an extended progenitor is favored by the early-time observations.

Further evidence for this scenario can be sought by analyzing the temperature of the ejecta. Figure 9 shows the evolution of effective temperature for both models. There are no important differences in the effective temperature for $t \gtrsim 2$ days, contrary to what was suggested by Arcavi et al. (2011). In that paper, the authors estimated a black-body temperature of $\approx$ 7600 K from the spectrum of SN 2011dh at 2.8 days, and compared it with the effective temperature derived from an analytic expression of (Rabinak & Waxman 2011, RW11 hereafter) that strongly depends on the progenitor radius, and less strongly on other parameters. Assuming a radius of $\sim 10^{13}$ cm at $t = 2.8$ days after the explosion, the predicted temperature is $T_{\rm eff} \approx 17000$ K. This discrepancy is one of the main arguments they used to rule out an extended progenitor, such as a YSG. On the contrary, our numerical calculations give values of $T_{\rm eff} =$ 7730 K and 7690 K at this epoch for compact and extended progenitor, respectively, which is compatible with the value derived from the spectrum.

An additional model named He4R270NH is shown in Figure 9 (dotted line). This model is similar to He4R270, but with larger helium mass fraction in the envelope of $Y \approx 1$, i.e. essentially hydrogen-free. One can see that the presence of H in the envelope of the extended progenitor (model He4R270) improves the agreement with the observation by reducing the temperature, as compared with a model where no H is included (model He4R270NH). The composition of the envelope thus plays an important role in the determination of the effective temperature.

For comparison, Figure 9 also shows the behavior of $T_{\rm eff}$ calculated using equation (13) of RW11 for the cases of compact and extended progenitors. The adopted radii are the same as those employed for the hydrodynamical calculations, i.e. $R = 2.4\,R_\odot$ and $R = 270\,R_\odot$. Note that only at very early times do the analytic models agree with the hydrodynamical calculations. At later times the agreement breaks down. This could be partially due to the effect of recombination in the ejecta which is not considered in expression (13) of RW11. Another possible reason for the disagreement could be differences in the initial density structures between both formulations (see Figure 1 for our initial density profile). A more detailed study is needed to clarify the origin of the discrepancy, but that goes beyond the scope of the present work. In any case, it is important to bear in mind that the analytic expressions were applied at an epoch ($\approx$ 2.8 days) that could be outside their validity range.

In any case, the $T_{\rm eff}$ is not directly comparable with the black-body temperature derived from the spectrum. A more direct comparison can be done using the color temperature ($T_{\rm C}$). Following the prescription of Ensman & Burrows (1992) we estimated $T_{\rm C}$ as the temperature at the "thermalization" depth[1], which led to values of 8500 K and 8300 K at 2.8 days for models He4 and He4R270, respectively. Although these values are somewhat higher than the value estimated from the spectrum, the discrepancy is not important given the uncertainties in the time of explosion ($\sim$ 0.6 day) and in the estimations of the color temperatures. Because of the small differences in temperature found at $t \sim 2$ days between compact and expended progenitors, the available temperature measurement is not a suitable discriminator between these scenarios.

Finally, we analyzed whether it is possible to improve the comparison between models and early observations assuming different values of the progenitor radius than that inferred for the YSG star. Figure 10 shows the bolometric (left panel) and g'-band (right panel) LCs for models with progenitor radii of 50, 100, 150 and 200 $R_\odot$. All of these configurations have the same He core taken from the He4 model, and they were constructed in a similar way as He4R270, i.e.smoothly attaching an H-rich envelope to the core (see Figure 1). We denote these models as He4R50, He4R100, He4R150 and He4R200. As seen from the figure, it is clear that models with $R \approx 200$ $R_\odot$ are more consistent with the early-time data. This finding is not affected by the systematic uncertainty in the luminosity that would arise from an error of 1 Mpc in the distance.

We conclude this analysis by claiming that a progenitor with radius similar to that of a YSG star, as suggested from pre-SN detections, is compatible with the early observations of SN 2011dh. Moreover, we find that radii much smaller than 200 $R_\odot$ fail to reproduce the observations.

4. DISCUSSION

4.1. *Single versus binary progenitor*

SNe IIb require the hydrogen-rich envelope of the progenitor star to be almost completely removed before the explosion. Two alternative mechanisms of envelope removal have been proposed to explain the progenitors of SNe IIb, Ib, and Ic, thereby called "stripped-envelope SNe": (1) strong stellar winds in massive single stars, and (2) mass transfer in close binary systems. In the first scenario a very massive star with a main sequence mass $\gtrsim 30\,M_\odot$ is required for the mass-loss rate to be large enough (Heger et al. 2003; Georgy et al. 2009). This type of star has a He core mass $\gtrsim 8\,M_\odot$ previous to the explosion. The upper limit of the main-sequence mass may be even larger according to recent stellar wind mass-loss rates (see Bouret et al. 2005; Eldridge & Vink 2006; Fullerton et al. 2006). In the binary scenario, less massive stars are allowed with He core masses prior to the explosion in the range of 3–6 $M_\odot$ (Podsiadlowski et al. 1993; Yoon et al. 2010). In the previous section we showed that such He-core mass range is in very good agreement with the observations of SN 2011dh.

To further test the possibility of a single-star progenitor, we calculated a model based on a progenitor with main sequence mass of 25 $M_\odot$ which forms a He core of 8 $M_\odot$ previous to the explosion (we call this model He8). In Figures 6 and 7 we show the LC and $v_{\rm ph}$, respectively, for model He8 using the same ^{56}Ni mass and distribution as found for the He4 model of section 3.1 but with a larger explosion energy of $E = 2$ foe in order to reproduce the peak luminosity. Clearly, this model does not agree well with the observations. While decreasing the explosion energy can improve the match to the expansion velocities, it would worsen the fit to the LC irrespective of the ^{56}Ni mixing assumed. Note that the timing of the second peak imposes an important constraint on the He core mass. More massive helium stars reach the LC maximum at later times because the heat produced by radioactive decays takes longer to diffuse out. The He8 model is too massive to produce the second maximum at ≈ 20 days as observed for SN 2011dh, even assuming the most extreme ^{56}Ni mixing.

---

[1] The "thermalization" depth is calculated as the layer where $3\,\tau_{\rm abs}\,\tau_{\rm sct} \approx 1$, where $\tau_{\rm sct}$ is the optical depth for scattering and $\tau_{\rm abs}$ is the optical depth for absorption.

This situation cannot be remedied by assuming a different distance to M51 within the uncertainty of 1 Mpc. This would move all the LC points systematically upward or downward by 0.12 dex, but it would not change the shape of the LC, i.e. its width and peak timing. Therefore our hydrodynamical modeling indicates that the He core mass must be lower than 8 $M_\odot$, which favors a binary origin for SN 2011dh.

Recently it has been suggested that the binary channel is preferred to explain most of the stripped-envelope SNe. This is supported for example by population studies compared with the observed rates of SNe (Eldridge et al. 2008; Smith et al. 2011). In the case of SNe IIb the binary picture is further strengthened for two reasons: Firstly, stellar evolution of single stars requires a precise fine tuning of the initial parameters to leave a thin H envelope previous to the explosion. This is much more naturally explained in a binary context (Podsiadlowski et al. 1993; Woosley et al. 1994; Yoon et al. 2010). Secondly, the detection of the binary companion in the case of the type IIb SN 1993J, and possibly also in the case of SN 2001ig. A K0 supergiant star was identified as the progenitor of SN 1993J (Aldering et al. 1994). However, the pre-SN photometry showed an excess in the UV and B bands that was associated with a blue companion star. Approximately a decade after the explosion the blue supergiant companion was confirmed (Maund et al. 2004; Maund & Smartt 2009). In the case of SN 2001ig, a possible companion star was reported by Ryder et al. (2006).

The observed pre-SN photometry of SN 2011dh fits well the spectral energy distribution (SED) of a single YSG star (Maund et al. 2011; Van Dyk et al. 2011). Therefore, for the binary sceneario to apply, the companion flux should have no appreciable effect on the pre-SN photometry. We have performed binary evolution calculations to test the possibility of systems that are compatible with the pre-SN observations. For this purpose, we employed the interacting-binary code developed by Benvenuto & De Vito (2003). The code was initially constructed for low-mass systems and recently extended to compute the evolution of massive stars by including nuclear reactions until the end of oxygen burning. Further details of these calculations are presented in our companion paper Benvenuto et al (2012).

Figure 11 shows the evolutionary tracks in the H-R diagram for both components of a binary system composed of a primary (donor) star with an initial mass of 16 $M_\odot$, a secondary (accreting) star of 10 $M_\odot$, and an initial orbital period of 150 days. The conservative mass-transfer case ($^2\beta = 1$) is shown in the left panel of the figure, where all the matter lost by the primary star is accreted onto the secondary. The right panel shows a non-conservative case with an accretion efficiency of 25% ($\beta = 0.25$). With this configuration, independently of the adopted value of β, the primary star ends its evolution within the region of the H-R diagram defined by the pre-SN photometry and its uncertainty. Also note that the mass of the primary star prior to the explosion is $\approx 4 M_\odot$, which is consistent with the hydrodynamical modeling presented in the previous section.

Furthermore, in all the above calculations some hydrogen remains in the envelope of the primary star at the moment of the explosion with a similar mass of $\approx 4 \times 10^{-3} M_\odot$. This H mass is high enough to be detected in the spectra and therefore it is consistent with the SN IIb classification (Dessart et al. 2011).

To study the effect of the secondary on the pre-explosion photometry we used atmosphere models of Kurucz (1993)[3] for the corresponding $T_{\rm eff}$, surface gravity and radius of both binary components to compute synthetic magnitudes through the observed HST bandpasses. As can be seen in Figure 11, the secondary star is significantly bluer than the primary at the time of explosion. Thus, the largest contribution to the flux of the system from the secondary is in the bluest band, F336W. For both values of β the contribution of the secondary in the rest of the bands is $< 4\%$. In the conservative case ($\beta = 1$) the secondary would increase the flux of the system in the F336W band by 50%, producing a marginal 1.5 σ detection, considering the measurement uncertainty in this band. In the non-conservative case with $\beta = 0.25$ the contribution of the secondary in the bluest band is only of 30% of the total flux which falls well inside the photometric uncertainty (0.6 σ).

If the binary scenario really applies to the case of SN 2011dh, the companion star should be recovered in future observations, when the SN becomes faint enough. From the synthetic photometry described above and assuming a distance to M51 of 7.1 Mpc (Takáts & Vinkó 2006) and no host-galaxy extinction, the expected brightness of the secondary in the F336W band is 24.9 mag and 24.2 mag for $\beta = 0.25$ and $\beta = 1$, respectively. In the redder bands, the brightness lies within 26–27 mag. A search for the secondary star using the HST when the SN fades enough is feasible and can serve to ultimately test the binary scenario.

4.2. *Compact versus extended progenitor*

In the literature, a more compact progenitor has been suggested for SN 2011dh than the YSG object detected at the SN position (Arcavi et al. 2011; Soderberg et al. 2012; Van Dyk et al. 2011). This was based on (1) a comparison between the early decline rate in the LC of SN 1993J and SN 2011dh, (2) an incompatibility between the temperature derived from an early-time spectrum and that estimated from analytic expressions for an extended object, and (3) large shock velocity derived from radio observations.

Regarding the first point, while it is true that SN 1993J showed a slower decline during the cooling phase as com-

---

[2] β represents the fraction of material lost by the donor star that is accreted by the secondary.

[3] The Kurucz stellar atmospheres atlas was downloaded from `http://www.stsci.edu/hst/observatory/cdbs/k93models.html`

pared with SN 2011dh, this can be explained by the difference in size of the proposed progenitors. SN 1993J was suggested to have a red supergiant progenitor with a radius of $\approx 600R_\odot$ (Maund et al. 2004, $\log L/L_\odot = 5.1$ and $\log T_{\rm eff} = 3.63$), whereas the YSG star that was proposed as the progenitor of SN 2011dh has a smaller radius of $\approx 200R_\odot$. To test this statement we calculated a model for SN 1993J based on the He4 progenitor with an envelope attached to make L and $T_{\rm eff}$ consistent with the pre-explosion photometry of SN 1993J (see Maund et al. 2004). Figure 12 shows a comparison between our model and the observations of SN 1993J (Richmond et al. 1994) assuming the explosion date was 1993 March 27.5 UT. An explosion energy of $E = 1.2$ foe and a ^{56}Ni mass of 0.084 $M_\odot$ were used in this simulation. Such values are consistent with those adopted by Shigeyama et al. (1994). We also show the He4R270 model and the observations of SN 2011dh for a clear comparison between both SNe and models. From the figure it is clear that the difference in radius is enough to explain the difference in decline rate of the early light curves between both SNe.

With respect to the temperature discrepancy of the second point above, using hydrodynamical models in § 3.2 we did not find any incompatibility with the spectrum temperature at $t \approx 2.8$ days when assuming an extended object. Note that our models show that the differences in temperature for $t \gtrsim 2$ days between compact and extended progenitors are too small to discriminate between these scenarios. In our modeling we are able to determine the radius and thus set a lower limit of about 200 $R_\odot$ (see Section 3.2) based on the comparison with the early LC and not with the temperature.

Regarding the issue of the radio properties, the shockwave velocity appears to be too high for an extended object based on the picture presented by Chevalier & Soderberg (2010). However, the connection between the shock velocity and the physical radius of the progenitor is not direct and relies on several assumptions (see Soderberg et al. (2012); Krauss et al. (2012)). Therefore, we think that this argument alone cannot be used to rule out the extended progenitor scenario. Moreover, it is worth noting that the mass-loss rate estimated from radio observations by Krauss et al. (2012) is compatible with a YSG progenitor and that no variability in the radio light curve, as has been observed for some compact SNe IIb (Ryder et al. 2004; Soderberg et al. 2006), was reported to date.

5. CONCLUSIONS

We have calculated a set of hydrodynamical models applied to stellar-evolution progenitors in order to study the nature of SN 2011dh. Comparing our models with the observed bolometric LC during the second peak and with line expansion velocities we found that a progenitor with He core mass of 3.3–4 $M_\odot$, an explosion energy of $6 - 10 \times 10^{50}$ erg, and a ^{56}Ni mass of ≈ 0.06 $M_\odot$ reproduce very well the observations assuming a distance of 7.1 Mpc to M51. This type of model is consistent with a main sequence mass between 12 and 15 $M_\odot$. Remarkably, the range of mass found with our hydrodynamical modeling is in very good agreement with the estimates from two other independent methods, i.e. pre-SN imaging and stellar population analysis. This is different from the situation generally encountered for SNe IIP where LC modeling estimates main sequence masses that are higher up to a factor of two than those estimated from pre-SN imaging (Utrobin & Chugai 2008; Smartt 2009).

We have studied the effect of the progenitor radius on the early LC and temperature evolution. We found that a progenitor with radius similar to that of the YSG star detected in the pre-SN images is compatible with the early observations of SN 2011dh without contradiction with the temperature that is derived from the spectrum, as opposed to what Arcavi et al. (2011) found using analytic models. Furthermore, progenitors with radii $< 200\,R_\odot$ fail to reproduce the early g'-band LC. Although our hydrodynamical models show differences in the temperature evolution between extended and compact progenitors, these differences are less marked than those predicted by analytic expressions and they are almost unnoticeable for $t \gtrsim 2$ days. Therefore, the spectrum temperature at $t \approx 2.8$ days is not useful in this case to discriminate between compact and extended progenitors.

We have tested *and ruled out* progenitors with He core masses $\gtrsim 8M_\odot$ which correspond to $M_{\rm ZAMS} \gtrsim 25\,M_\odot$. Considering the limitations at such stellar masses of single-star winds to expel the H-rich envelope almost entirely, as required for SNe IIb, this result is in favor of a binary origin for SN 2011dh.

We have also performed binary evolution calculations with mass transfer to test the possibility of systems that are compatible with the pre-SN observations of SN 2011dh. We have shown that a system with 16 $M_\odot$ + 10 $M_\odot$ and an initial period of 150 days predicts that the primary star ends its evolution in the H-R diagram at the right position as compared with the YSG star detected in the pre-SN images (Maund et al. 2011; Van Dyk et al. 2011). Furthermore, the He mass of the primary at the end of the evolution was $\approx 4M_\odot$, which is consistent with our hydrodynamical modeling. The binary evolution calculations further predict that some hydrogen mass of $\approx 4 \times 10^{-3}M_\odot$ is left in the envelope of the primary star, which is required to produce a SN IIb.

To test the binary scenario we have studied the effect of the putative companion star on the pre-explosion photometry in comparison with the observations. Because the secondary star is predicted to be much hotter than the primary star, we found that the largest effect appears in the blue and UV filters. The contribution of the secondary to the flux in the F336W band, however, is marginal, at the 1.5 σ level. The contribution is further decreased to the 0.6 σ level when non-conservative mass accretion is considered. However, our predictions can be tested in a few years time by a search for a blue object at the location of the SN.

This research has been supported in part by the Grant-in-Aid for Scientific Research of MEXT (22012003 and 23105705) and JSPS (23540262) and by World Premier International Research Center Initiative, MEXT, Japan. SB is partially supported by the PRIN-INAF 2009 with the project "Supernovae Variety and Nucleosynthesis Yields".

REFERENCES

Aldering, G., Humphreys, R. M., & Richmond, M. 1994, AJ, 107, 662

Arcavi, I., Gal-Yam, A., Yaron, O., et al. 2011, ApJ, 742, L18

Arnett, D. 1996, Supernovae and Nucleosynthesis: An Investigation of the History of Matter, from the Big Bang to the Present, by D. Arnett. Princeton: Princeton University Press, 1996.

Benvenuto, O. G., & De Vito, M. A. 2003, MNRAS, 342, 50

Benvenuto, O., in preparation

Bersten, M. C., Benvenuto, O., & Hamuy, M. 2011, ApJ, 729, 61

Bietenholz, M. F., Brunthaler, A., Soderberg, A. M., et al. 2012, arXiv:1201.0771

Blinnikov, S. I., Eastman, R., Bartunov, O. S., Popolitov, V. A., & Woosley, S. E. 1998, ApJ, 496, 454

Blinnikov, S., Lundqvist, P., Bartunov, O., Nomoto, K., & Iwamoto, K. 2000, ApJ, 532, 1132

Bouret, J.-C., Lanz, T., & Hillier, D. J. 2005, A&A, 438, 301

Chevalier, R. A., & Soderberg, A. M. 2010, ApJ, 711, L40

Dessart, L., Hillier, D. J., Livne, E., et al. 2011, MNRAS, 414, 2985

Eldridge, J. J., & Vink, J. S. 2006, A&A, 452, 295

Eldridge, J. J., Izzard, R. G., & Tout, C. A. 2008, MNRAS, 384, 1109

Ensman, L., & Burrows, A. 1992, ApJ, 393, 742

Ergon, M., in preparation

Fullerton, A. W., Massa, D. L., & Prinja, R. K. 2006, ApJ, 637, 1025

Gal-Yam, A., Leonard, D. C., Fox, D. B., et al. 2007, ApJ, 656, 372

Filippenko, A. V. 1997, ARA&A, 35, 309

Filippenko, A. V. 1988, AJ, 96, 1941

Georgy, C., Meynet, G., Walder, R., Folini, D., & Maeder, A. 2009, A&A, 502, 611

Gilmozzi, R., Cassatella, A., Clavel, J., et al. 1987, Nature, 328, 318

Griga, T., Marulla, A., Grenier, A., et al. 2011, Central Bureau Electronic Telegrams, 2736, 1

Hachisu, I., Matsuda, T, Nomoto, K., & Shigeyama, T. 1991, ApJ 368, L27

Hachisu, I., Matsuda, T, Nomoto, K., & Shigeyama, T. 1994, A&AS 104, 341

Hammer, N. J., Janka, H.-T., Muller, E. 2010, ApJ, 714, 1371

Heger, A., Fryer, C. L., Woosley, S. E., Langer, N., & Hartmann, D. H. 2003, ApJ, 591, 288

Hix, W. R., & Thielemann, F.-K. 1996, ApJ, 460, 869

Hix, W. R., & Thielemann, F.-K. 1999, ApJ, 511, 862

Iwamoto, K., Young, T.R., Nakasato, N., Shigeyama, T., Nomoto, K., Hachisu, I., Saio, H. 477, 865

Joggerst, C. C., Almgren, A., & Woosley, S. E. 2010, ApJ, 723, 353

Kawabata, K. S., Maeda, K., Nomoto, K., et al. 2010, Nature, 465, 326

Krauss, M. I., Soderberg, A. M., Chomiuk, L., et al. 2012, arXiv:1201.0770

Kurucz, R. 1993, ATLAS9 Stellar Atmosphere

Maund, J. R., Fraser, M., Ergon, M., et al. 2011, ApJ, 739, L37

Maund, J. R., Smartt, S. J., Kudritzki, R. P., Podsiadlowski, P., & Gilmore, G. F. 2004, Nature, 427, 129

Maund, J. R., & Smartt, S. J. 2009, Science, 324, 486

Murphy, J. W., Jennings, Z. G., Williams, B., Dalcanton, J. J., & Dolphin, A. E. 2011, ApJ, 742, L4

Nomoto, K., Suzuki, T., Shigeyama, T., et al. 1993, Nature, 364, 507

Nomoto, K., & Sugimoto, D. 1972 Prog. Theor. Phys. 48, 46

Nomoto, K. 1974 Prog. Theor. Phys. 52, 453

Nomoto, K.,& Hashimoto, M. 1988, Phys. Rep., 163, 1

Podsiadlowski, P., Hsu, J. J. L., Joss, P. C., & Ross, R. R. 1993, Nature, 364, 509

Rabinak, I., & Waxman, E. 2011, ApJ, 728, 63

Richmond, M. W., Treffers, R. R., Filippenko, A. V., et al. 1994, AJ, 107, 1022

Ryder, S. D., Sadler, E. M., Subrahmanyan, R., et al. 2004, MNRAS, 349, 10

Ryder, S. D., Murrowood, C. E., & Stathakis, R. A. 2006, MNRAS, 369, L32

Shigeyama, T., Suzuki, T., Kumagai, S., et al. 1994, ApJ, 420, 341

Shigeyama, T., Nomoto, K., Tsujimoto, T., & Hashimoto, M.-A. 1990, ApJ, 361, L23

Silverman, J. M., Filippenko, A. V., & Cenko, S. B. 2011, The Astronomer's Telegram, 3398, 1

Smartt, S. J. 2009, ARA&A, 47, 63

Smartt, S. J., Eldridge, J. J., Crockett, R. M., & Maund, J. R. 2009, MNRAS, 395, 1409

Smith, N., Li, W., Filippenko, A. V., & Chornock, R. 2011, MNRAS, 412, 1522

Soderberg, A. M., Chevalier, R. A., Kulkarni, S. R., & Frail, D. A. 2006, ApJ, 651, 1005

Soderberg, A. M., Margutti, R., Zauderer, B. A., et al. 2012, ApJ, 752, 78

Sugimoto, D., & Nomoto, K. 1980, Space Sci. Rev., 25, 155

Swartz, D. A., Sutherland, P. G., & Harkness, R. P. 1995, ApJ, 446, 766

Takáts, K., & Vinkó, J. 2006, MNRAS, 372, 1735

Tanaka, M., et al. 2009, ApJ, 692, 1131

Thielemann, F.-K., Nomoto, K., & Hashimoto, M.-A. 1996, ApJ, 460, 408

Van Dyk, S. D., Li, W., Cenko, S. B., et al. 2011, ApJ, 741, L28

Utrobin, V. P., & Chugai, N. N. 2008, A&A, 491, 507

Walmswell, J. J., & Eldridge, J. J. 2012, MNRAS, 419, 2054

Woosley, S. E., Eastman, R. G., Weaver, T. A., & Pinto, P. A. 1994, ApJ, 429, 300

Woosley, S. E. & Weaver, T. A. . Massive stars, supernovae, and nucleosynthesis. Supernovae: Les Houches, session LIV, 1990

Yoon, S.-C., Woosley, S. E., & Langer, N. 2010, ApJ, 725, 940

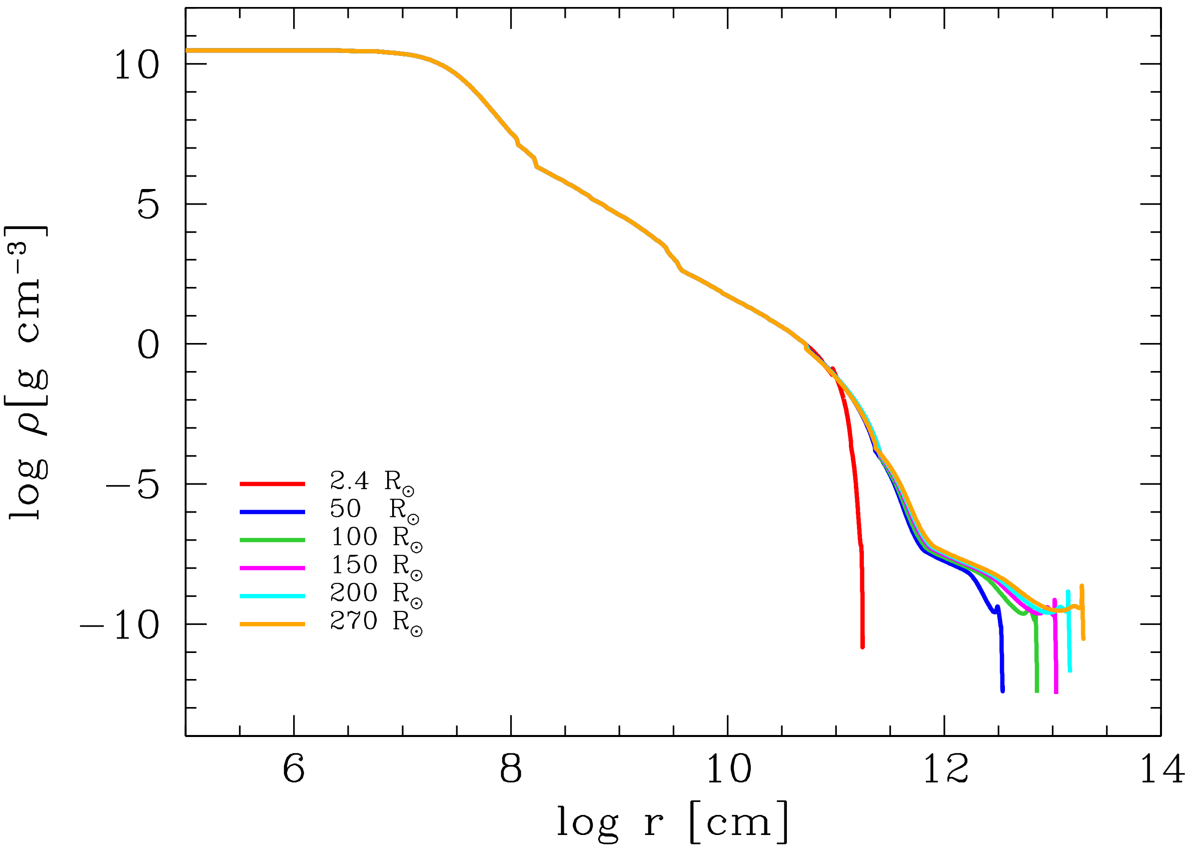

Fig. 1.— The initial density distributions as a function of radius for model He4 (red line) and for models with different H-rich envelopes attached to the core of He4.

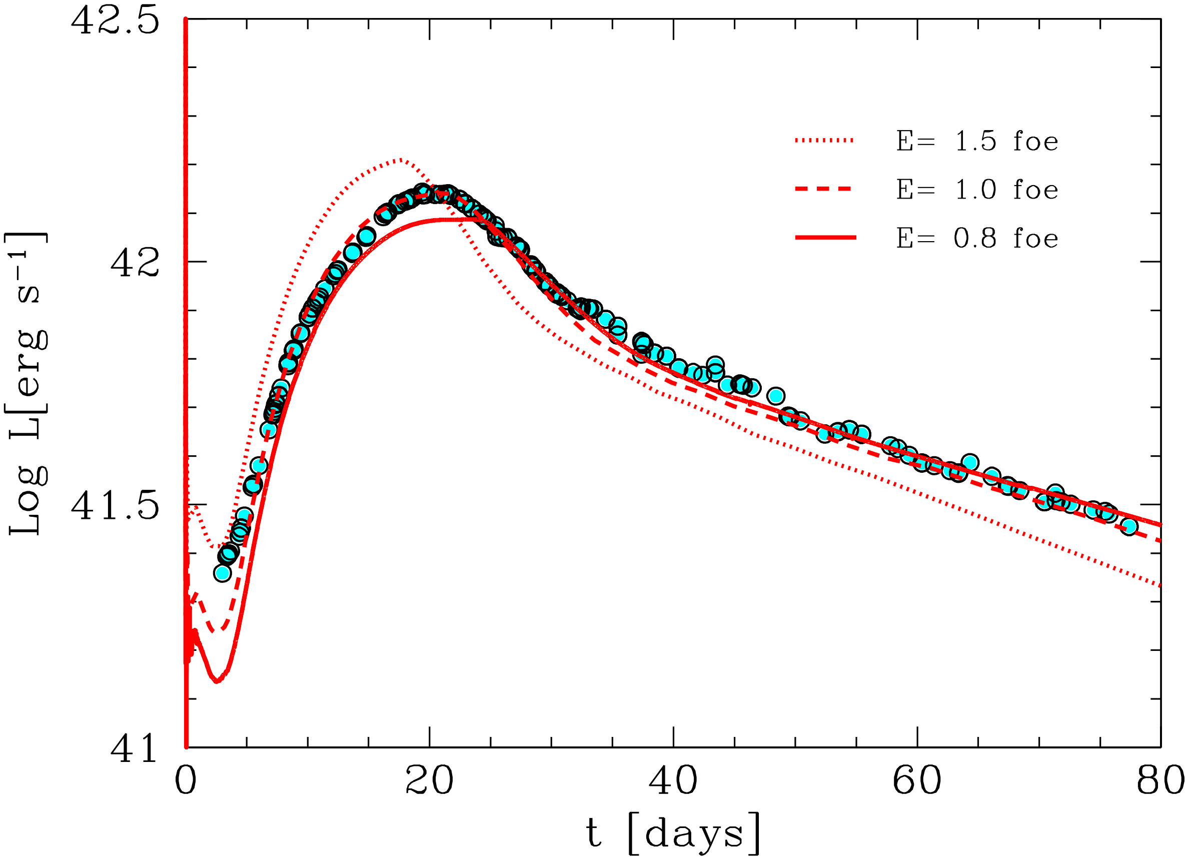

Fig. 2.— Sensitivity of the bolometric LC to changes in the explosion energy. The He4 initial model (see § 3.1) and three different values of the explosion energy, $E = 0.8, 1.0, 1.5$ foe, were used in these simulations. The observed bolometric LC of SN 2011dh (points) is shown for comparison.

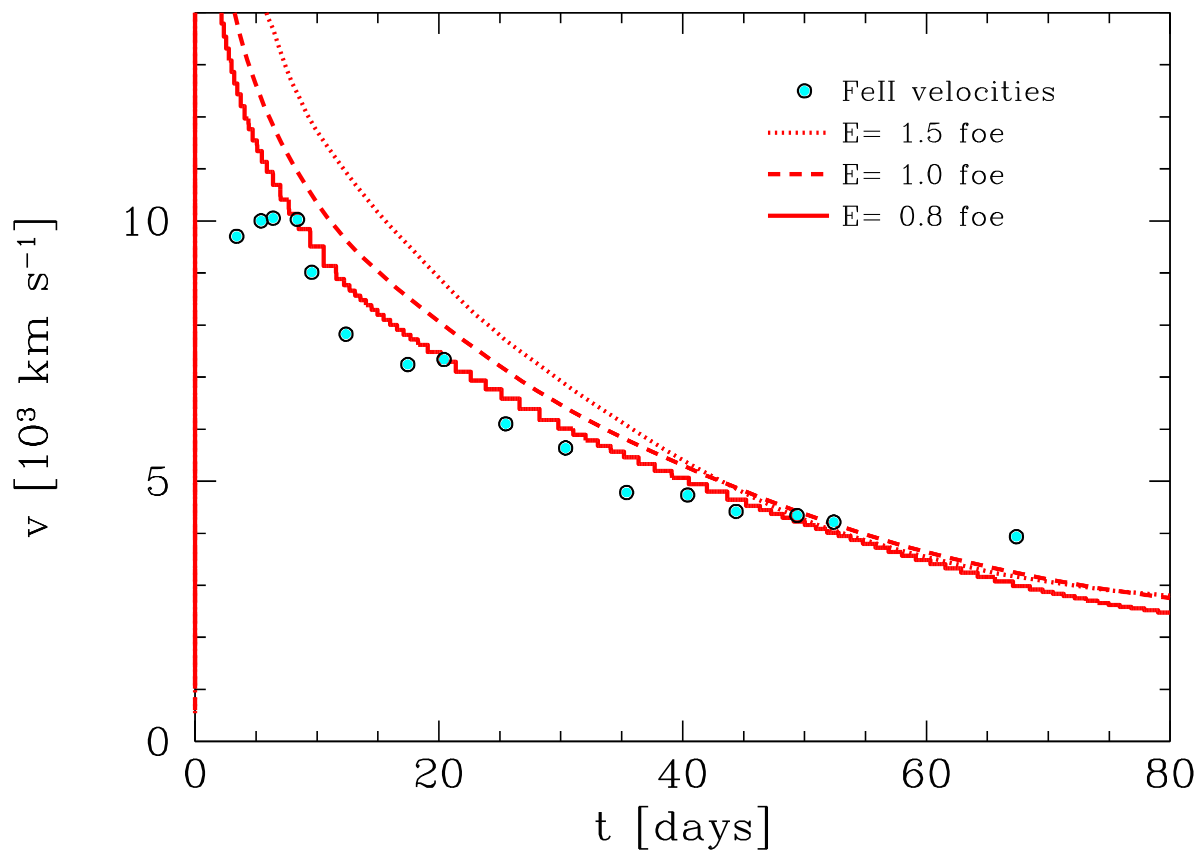

Fig. 3.— Sensitivity of the photospheric velocity evolution on the explosion energy. The He4 initial model (see § 3.1) and three different values of the explosion energy, $E = 0.8, 1, 1.5$ foe, were used in these simulations. Fe II line velocities measured from spectra of SN 2011dh (points) are shown for comparison.

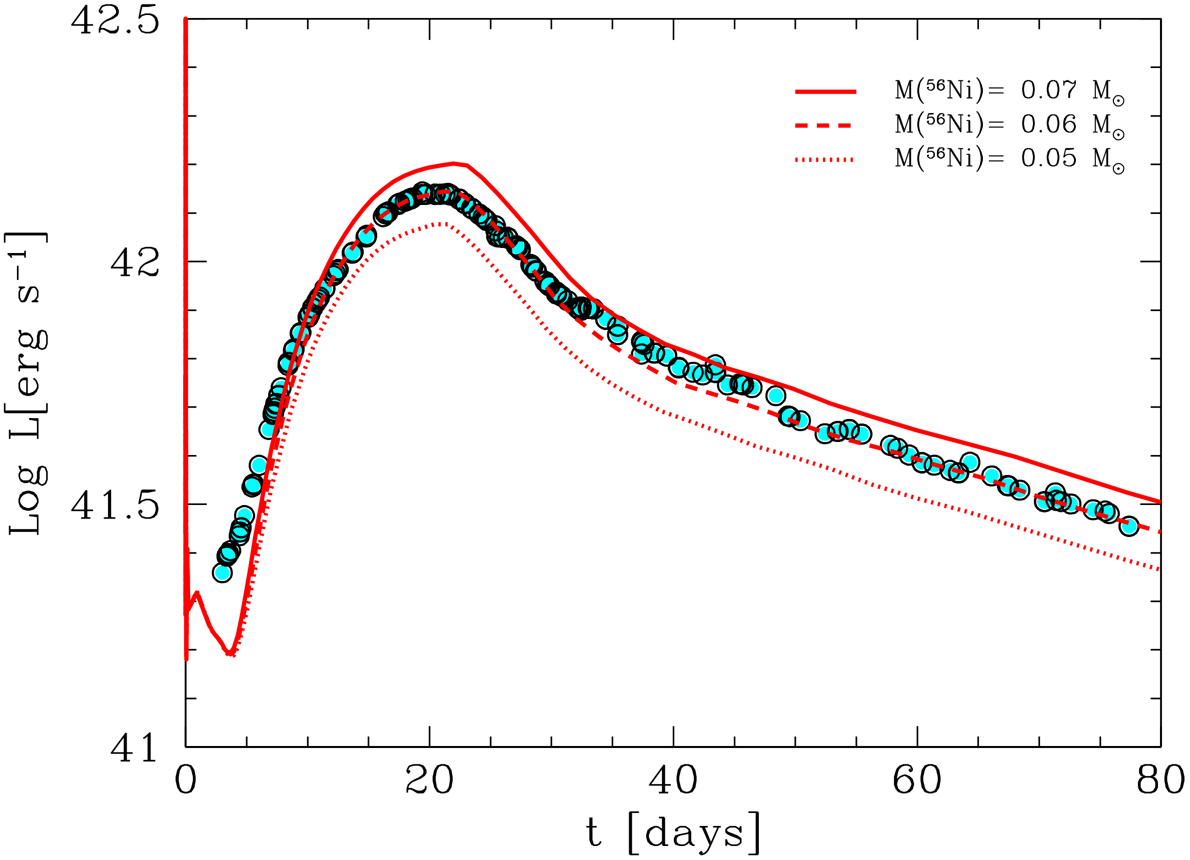

Fig. 4.— Sensitivity of the bolometric LC to changes in ^{56}Ni mass. The He4 initial model (see § 3.1) and three different values of the ^{56}Ni mass, ^{56}Ni mass $= 0.05, 0.06, 0.07\ M_\odot$, were used in these simulations. The observed bolometric LC of SN 2011dh (points) is shown for comparison.

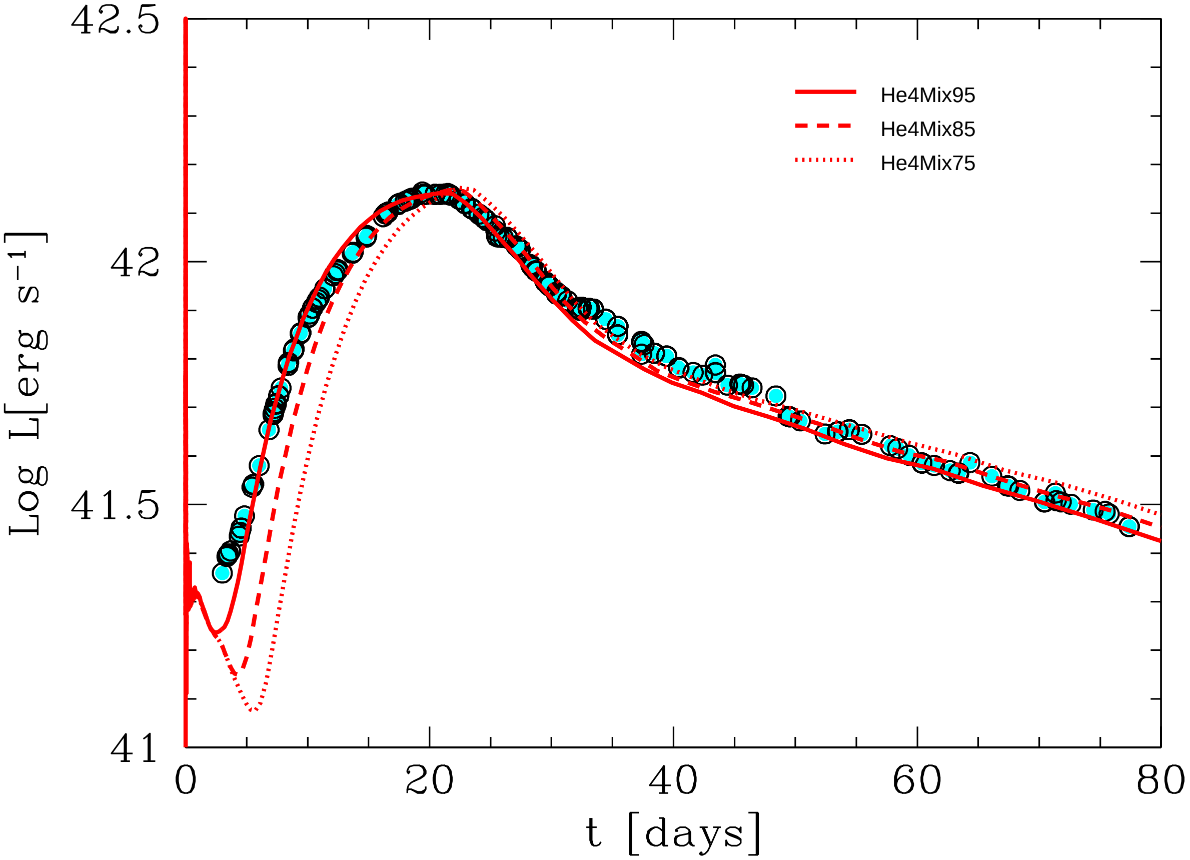

FIG. 5.— Sensitivity of the bolometric LC to changes in the ^{56}Ni distribution. The He4 initial model with ^{56}Ni mass= 0.06 $M_{\odot}$ (see § 3.1) and three different degrees of mixing, up to 75% (He4Mix75), 85% (He4Mix85), and 95% (He4Mix95) of the total initial mass, were used in these simulations. The observed bolometric LC of SN 2011dh (points) is shown for comparison.

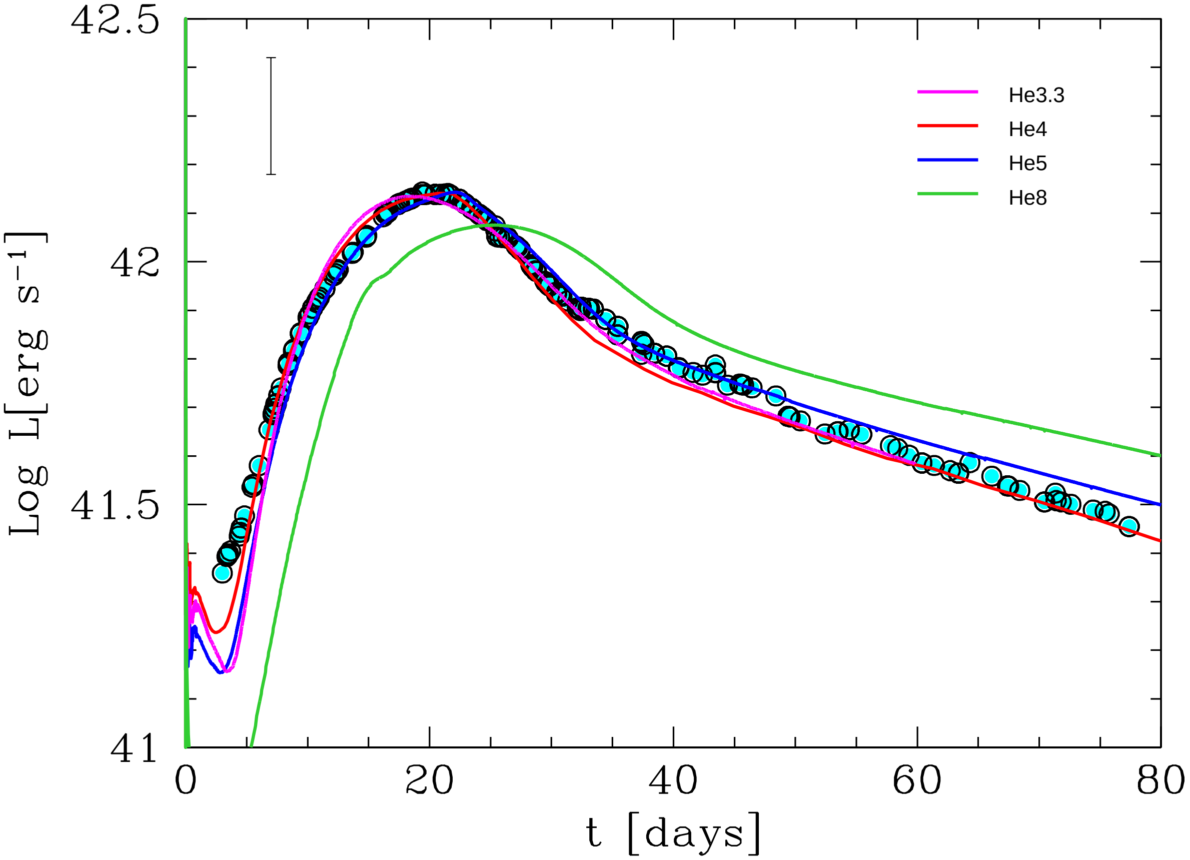

Fig. 6.— Observed bolometric LC of SN 2011dh (points) compared with the results of the LC calculations for models He3.3 (magenta solid line), He4 (red solid line) and He5 (blue solid line). An extra model, He8 (green solid line) is also included to show that larger helium core mass is not compatible with the observations. The error bar indicates the size of the systematic uncertainty in luminosity as derived from an uncertainty of 1 Mpc in the distance to M51. The physical parameters used in each simulation are given in Table 1.

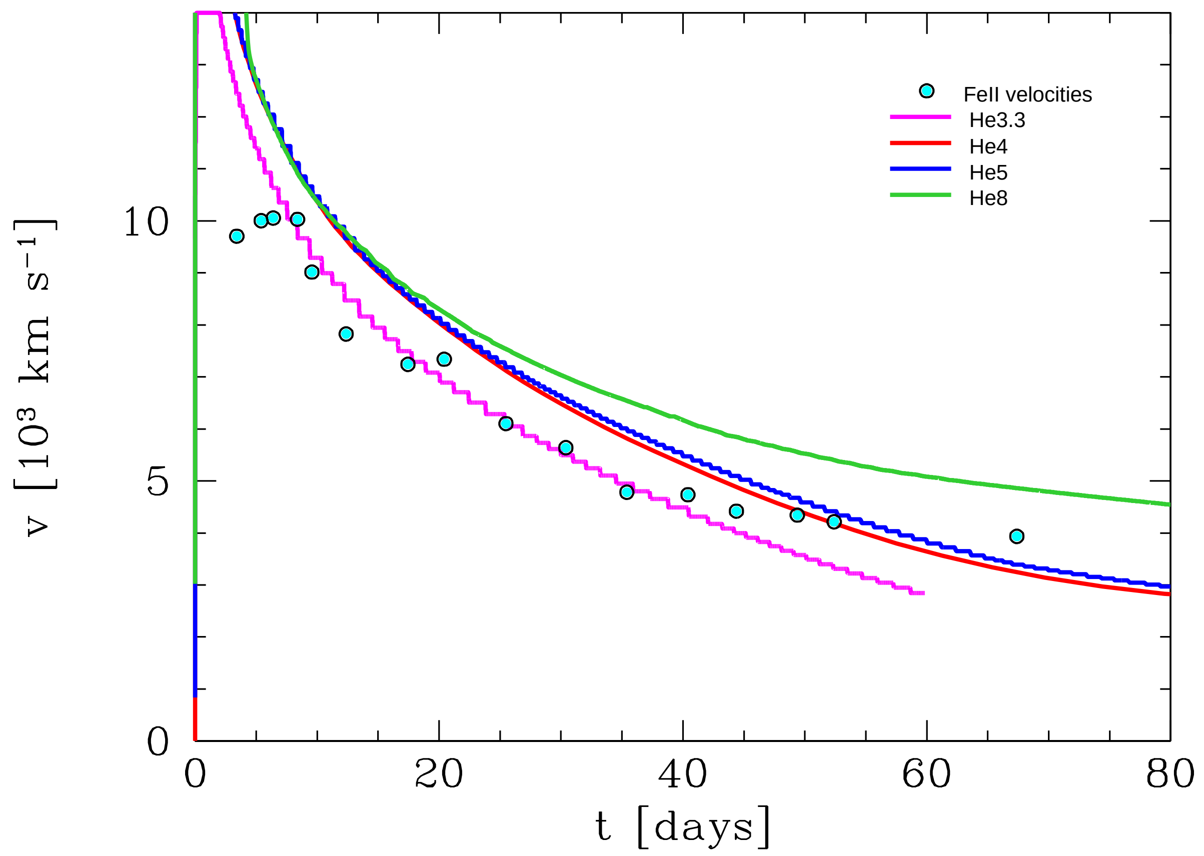

Fig. 7.— Evolution of the photospheric velocity for models He3.3 (magenta solid line), He4 (red solid line), He5 (blue solid line), and He8 (green solid line) compared with measured Fe II line velocities of SN 2011dh. The physical parameters used in each simulation are given in Table 1. Note that model with larger helium mass overestimate the observed velocities.

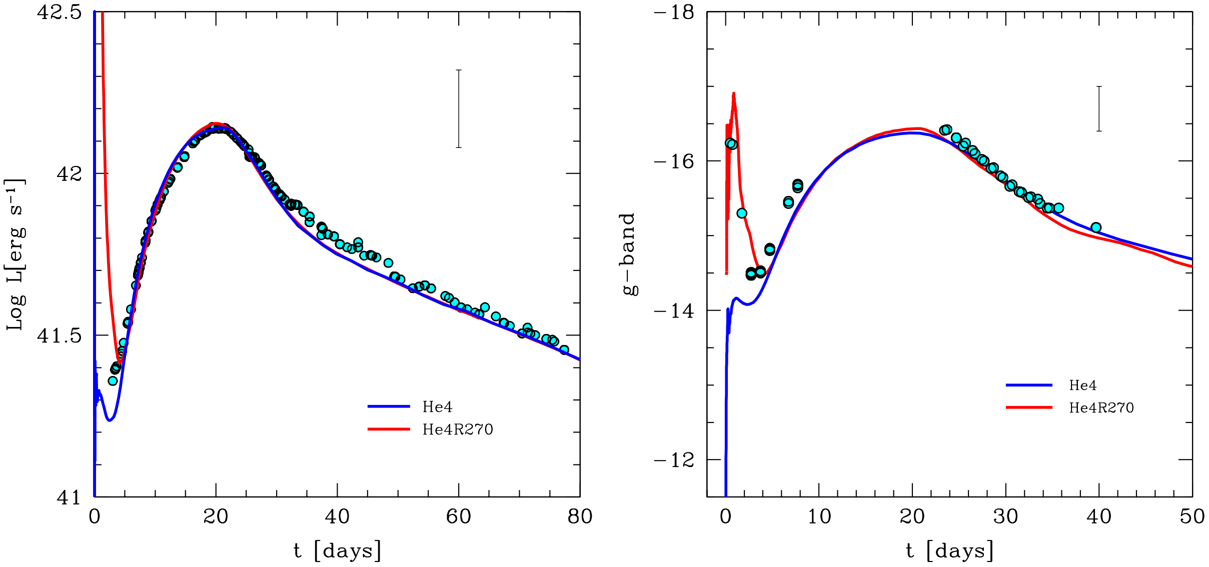

FIG. 8.— Observed and modeled bolometric LCs **(left panel)** and absolute g'-band LCs **(right panel)**. The dots show the observed bolometric LC from Ergon et al. (2012), and the g'-band LC from Arcavi et al. (2011). The blue solid lines show the results for the compact progenitor model He4. The red solid lines corresponds to an extended progenitor, He4R270, consistent with a YSG star as detected in pre-SN photometry of SN 2011dh. Clearly, the effect of the progenitor radius is only important before the radioactive material becomes the main source of radiative power. The larger radius is necessary to reproduce the early part of the g'-band LC. The error bars indicate the size of the systematic uncertainty that corresponds to an uncertainty of 1 Mpc in the distance to M51.

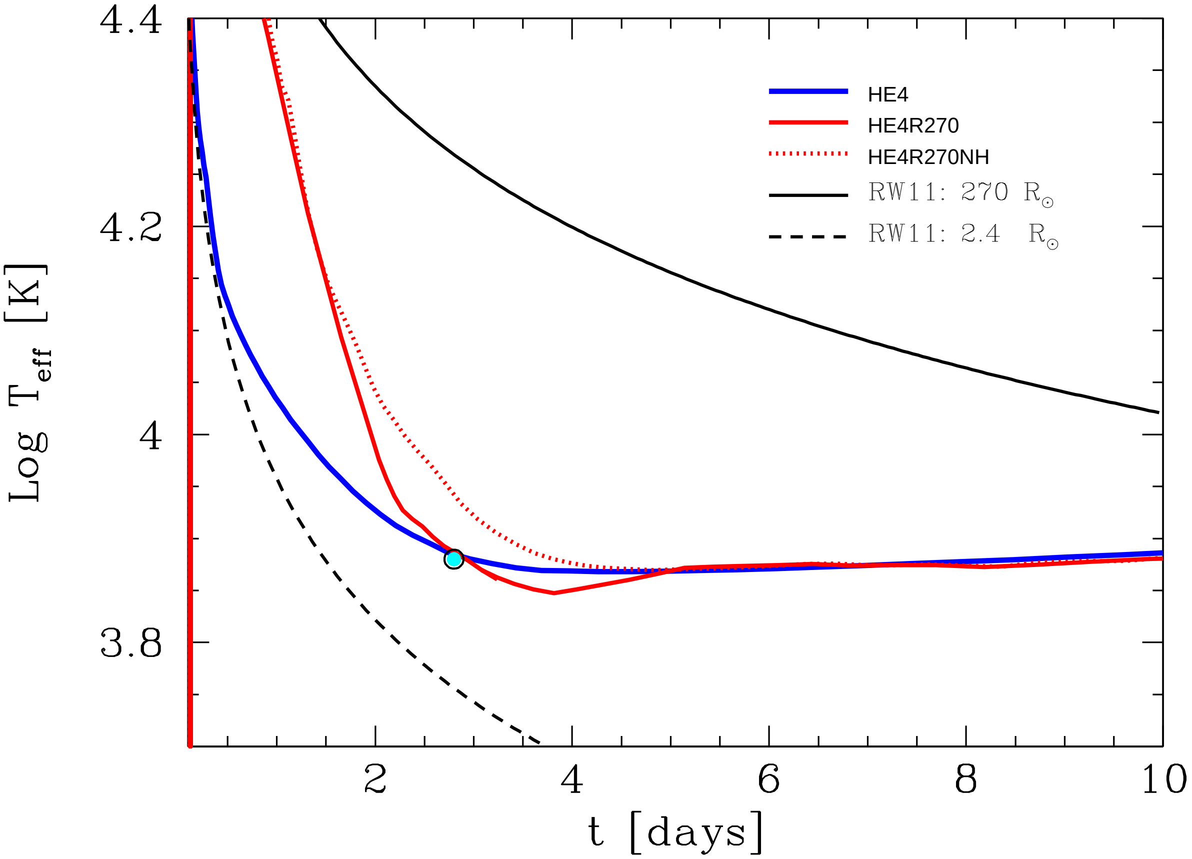

FIG. 9.— Time evolution of the effective temperature for the compact model He4 and the extended models He4R270 and He4R270NH (see § 3.2). The effective temperature calculated using the analytic expression of Rabinak & Waxman (2011) with $R = 270\,R_\odot$ (solid black line) and $R = 2.4\,R_\odot$ (dashed black line) are also shown. The black-body temperature (cyan dot) estimated from a spectrum of SN 2011dh obtained at 2.8 days is included for comparison.

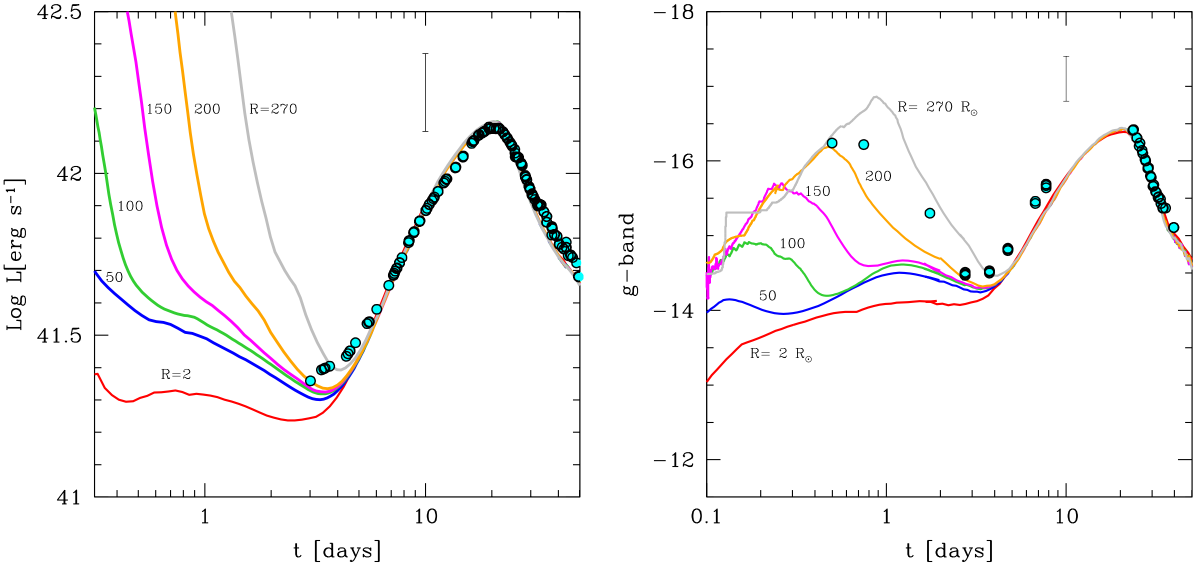

FIG. 10.— Bolometric LCs **(left panel)** and g'-band LCs **(right panel)** for models with the same explosion energy as our preferred model, but different initial radii. The observed bolometric LC (Ergon et al. 2012) and g'-band LC (Arcavi et al. 2011) of SN 2011dh (cyan dots) are shown for comparison in each panel. The error bars indicate the size of the systematic uncertainty that corresponds to an uncertainty of 1 Mpc in the distance to M51. The radius variation is accomplished by attaching essentially massless ($< 0.01\ M_\odot$) envelopes to the He4 model. Larger radii produce higher early luminosity for $t \lesssim 5$ days but no appreciable effect is seen at later times.

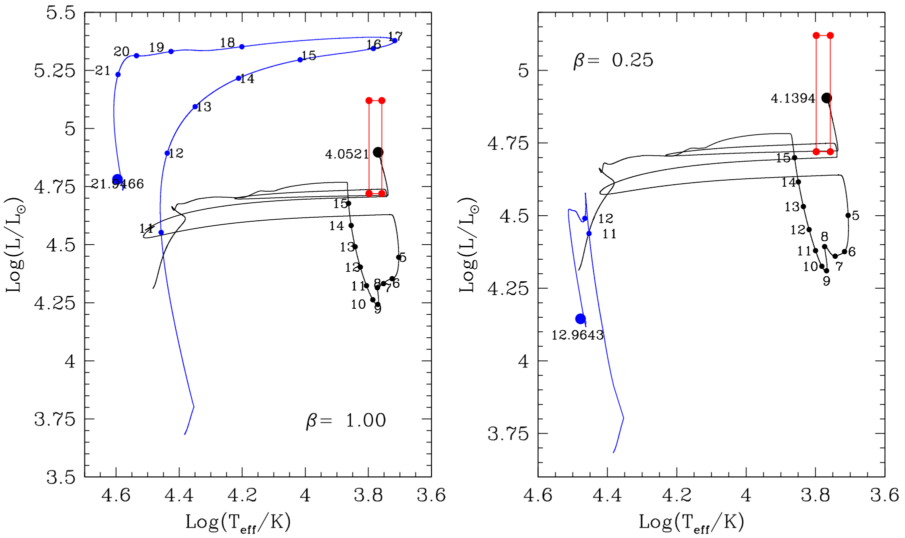

FIG. 11.— Evolutionary tracks in the Hertzsprung-Russell diagram for both components of a binary system with solar composition. The stars have $M_{\rm ZAMS}$ of 16 $M_\odot$ and 10 $M_\odot$ and an initial period of 150 days. **Left panel:** assuming conservative mass transfer ($\beta = 1$). **Right panel:** non-conservative mass transfer ($\beta = 0.25$). Labeled dots along the tracks indicate the masses of the stars (in solar masses) while mass-transfer by Roche-Lobe overflow occurs. The primary star (black line) ends its evolution with a mass $\approx 4\,M_\odot$ and with effective temperature and luminosity consistent with the YSG star detected in pre-SN images (red rectangle), independently of the value of β. However, the evolution of the secondary star (blue line) strongly depends on the assumed accretion efficiency. In the conservative case, the bolometric luminosity of both stars at the moment of the explosion of the primary star (big dot) is similar, while for $\beta = 0.25$ the secondary is ≈ 2 mag weaker than the primary at the end point.

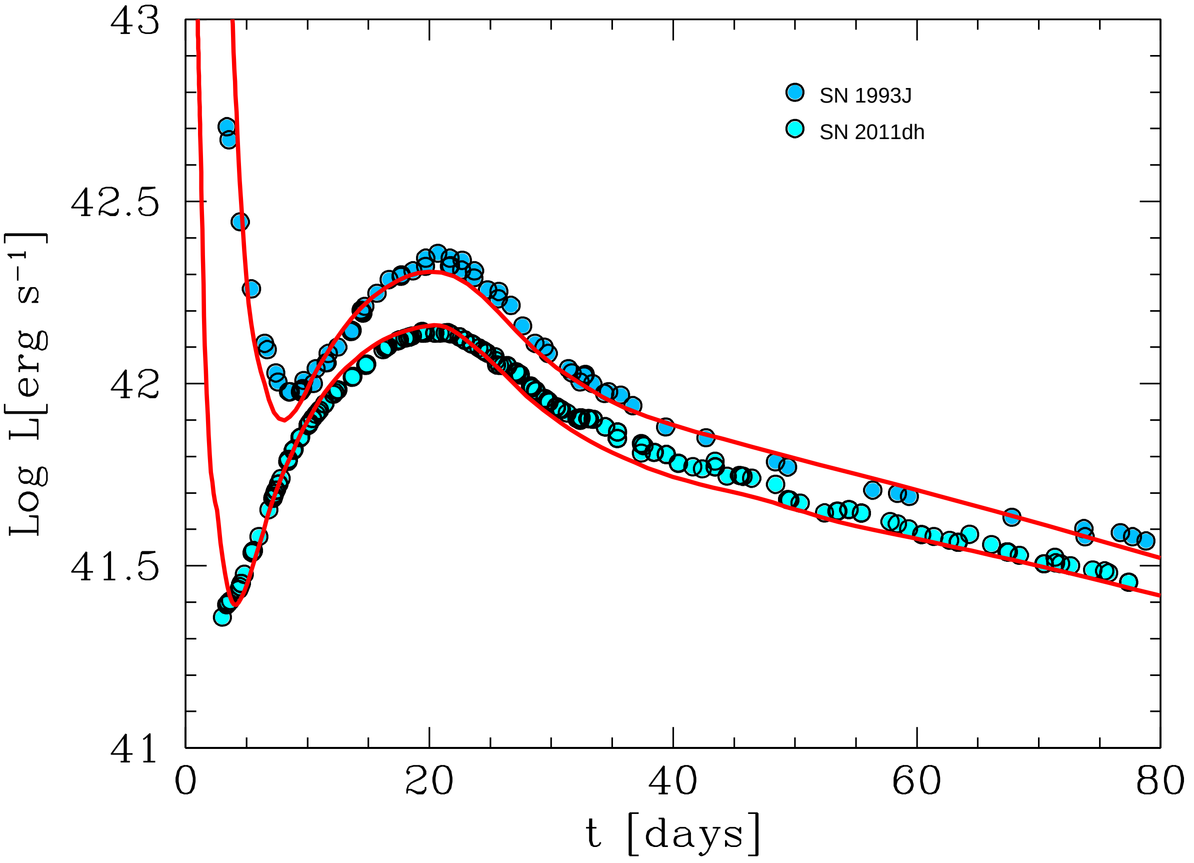

FIG. 12.— Comparison between theoretical bolometric LCs (solid lines) and observations (dots) for SN 1993J (Richmond et al. 1994) and SN 2011dh (Ergon et al. 2012). In both cases a progenitor was used with He core mass of 4 $M_{\odot}$. Envelopes of different radii were attached to the core to make L and $T_{\rm eff}$ consistent with pre-explosion imaging of each SN. The differences during the cooling phase are well explained as differences in the size of the progenitor while the differences in the main peak and tail are related with different different values of the explosion energy and ^{56}Ni mass.

TABLE 1
Physical parameters of the explosion models

Model	$M_{\rm ms}$[a] $[M_\odot]$	$M_{\rm He}$ $[M_\odot]$	$R_\star$ $[R_\odot]$	$M_{\rm cut}$ $[M_\odot]$	$M_{\rm ej}$ $[M_\odot]$	E [foe]	^{56}Ni mass $[M_\odot]$
He3.3	12	3.3	2.5	1.5	1.8	0.6	0.065
He4	15	4.	2.4	1.5	2.5	1.	0.06
He5	18	5.	1.8	1.6	3.4	1.2	0.065
He8	25	8.	1.3	1.8	6.2	2.	0.065

[a] Main sequence mass